frontiers | Frontiers in Coatings, Dyes and Interface Engineering

TYPE Mini Review
PUBLISHED 03 July 2024
DOI 10.3389/frcdi.2024.1417527

OPEN ACCESS

EDITED BY
Robert Wood,
University of Southampton, United Kingdom

REVIEWED BY
Noé López Perrusquia,
Polytechnic University of the Valley of Mexico, Mexico

*CORRESPONDENCE
Wenjun Cai,
caiw@vt.edu

RECEIVED 15 April 2024
ACCEPTED 11 June 2024
PUBLISHED 03 July 2024

CITATION
Lee JY and Cai W (2024), From fabrication to mechanical properties: exploring high-entropy oxide thin films and coatings for high-temperature applications.
Front. Coat. Dye In. 2:1417527.
doi: 10.3389/frcdi.2024.1417527

From fabrication to mechanical properties: exploring high-entropy oxide thin films and coatings for high-temperature applications

Jun Yeop Lee and Wenjun Cai*

Department of Materials Science and Engineering, Virginia Polytechnic Institute and State University, Blacksburg, VA, United States

High-entropy oxides (HEOs) containing five or more cations have garnered significant attention recently due to their vastly tunable compositional space, along with their remarkable physical and mechanical properties, exceptional thermal stability, and phase reversibility at elevated temperatures. These characteristics position HEOs as promising candidates for structural components and coatings in high-temperature applications. While much of the ongoing research on HEOs centers around understanding processing-structure relationships, there remains a dearth of knowledge concerning their mechanical properties, crucial for their prospective high-temperature applications. Whether in bulk form or as coatings, the efficacy of HEOs hinges on robust mechanical properties across a spectrum of temperatures, to ensure structural integrity, fracture resistance, and resilience to thermal stress. This review offers a succinct synthesis of recent advancements in HEO research, spanning from processing techniques to mechanical behaviors under extreme conditions. Emphasis is placed on three key aspects: (1) Investigating the influence of processing parameters on HEO crystal structures. (2) Analyzing the interplay between crystal structure and mechanical properties, elucidating deformation mechanisms. (3) Examining the mechanical behavior of HEOs under extreme temperatures and pressures. Through this review, we aim to illuminate the effective control of HEOs' unique structures and mechanical properties, paving the way for their future applications in extreme environments.

KEYWORDS

high-entropy oxides, thin film, coating, mechanical properties, crystal structure, deformation mechanism, high temperature

1 Introduction

High-entropy oxides (HEOs) have recently attracted significant interest due to their unique properties and adaptability to meet the rapidly evolving demands of technology, particularly under extreme service conditions (Musicó et al., 2020). HEOs are single-phase solid solutions with five or more different cations and anions, strategically designed to maximize configurational entropy (Toher et al., 2019; Akrami et al., 2021). This approach aims to counteract enthalpic driving forces, thereby reducing Gibbs free energy, especially at elevated temperatures where the entropy contribution becomes more significant, ultimately achieving thermodynamic phase equilibrium (Spurling et al., 2022). Within HEOs,

elements of varying sizes are uniformly distributed across the structure, leading to substantial sublattice disorder and marked lattice distortions (Sarkar et al., 2019; Oses et al., 2020). These distortions elevate the activation energy, thereby retarding diffusion (Usharani et al., 2020; Fu et al., 2021; Sun and Dai, 2021; Gao et al., 2022). This sluggish diffusion, coupled with rapid cooling, contributes to the stability of HEOs at room temperature (Kotsonis et al., 2023). The cocktail effect of HEOs, the synergistic interaction of cations, can lead to superior performance than predicted by the rule of mixtures (Wang, 2022; Nan et al., 2023), overcoming trade-offs between properties like stiffness and thermal conductivity at high temperatures (Braun et al., 2018). These unique structural characteristics of HEOs endow them with thermal and mechanical properties distinct from those of low-entropy oxides, including high hardness, stiffness, and temperature resistance (Albedwawi et al., 2021; Kotsonis et al., 2023).

HEOs exhibit remarkable structural stability, maintaining a single phase even under extreme temperatures (Sarkar et al., 2018; Dong et al., 2019; Ren et al., 2019; Zhao et al., 2019) and pressures (Chen et al., 2019; Cheng et al., 2019; Cheng et al., 2020; Yan et al., 2021; Yue et al., 2022). While enthalpy-driven phase separation may occur at high temperature, most HEOs can reversibly transition back to a single phase upon further temperature elevation (Rost et al., 2015; Bérardan et al., 2016; Chen et al., 2018; Sarkar et al., 2018; Dupuy et al., 2019; Nallathambi et al., 2023). The severe lattice distortion, combined with thermal stability, results in low thermal conductivity and high stiffness, beneficial for thermal barrier protection. The mechanical properties of HEOs are primarily attributed to the solid solution structure, which exhibits severe lattice distortion due to the diverse sizes of the cations (Ling and Yan, 1988; Hong et al., 2019; Bi et al., 2020; Ren et al., 2020; Song et al., 2021; Xue et al., 2022; Zhang et al., 2024). HEOs typically feature a fine grain size, resulting from sluggish diffusion, which is further refined by an increase in the number of elements and their concentrations (Bi et al., 2020; Zhu et al., 2021; Khan et al., 2021; Song et al., 2021; Zenkin et al., 2022). Other strengthening mechanisms for ceramics such as dispersion strengthening through secondary phase particles, work hardening, and strengthening through preferred crystallographic orientations should also apply to HEOs (Kirnbauer et al., 2019; Nallathambi et al., 2023).

Temperature and pressure play significant roles in controlling the structure and mechanical properties of HEOs (Lin et al., 2010; Rost et al., 2015; Cheng et al., 2019; Hong et al., 2019; Kirnbauer et al., 2019; Cheng et al., 2020; Rost et al., 2022; Yue et al., 2022; Liu X. et al., 2023; Fu et al., 2024). At low temperatures, the entropic term may not be sufficient to counterbalance the enthalpic term, potentially leading to phase separation (Hong et al., 2019; Rost et al., 2022; Liu X. et al., 2023). High pressure can trigger phase transformations and may alter or eliminate lattice slip systems, offering toughening mechanisms for ceramics (Lai et al., 2013; Cheng et al., 2019; Cheng et al., 2020; Pang et al., 2022; Yue et al., 2022). Furthermore, electronic states, oxygen vacancies, and localized lattice distortions are also susceptible to pressure effects (Cheng et al., 2019; Cheng et al., 2020), which will influence mechanical response in the end.

To expand the application of HEOs into more extreme environments, a deeper understanding of their structures and consequent mechanical properties is required. This review focuses on processing techniques for HEO oxide thin films and coatings, elucidates strengthening mechanisms and the impact of HEO structures, and explores their mechanical behavior at elevated temperatures from a structural perspective.

2 Survey of processing-structure-mechanical properties relationships of HEOs

A literature survey on the interplay between processing, structure, and mechanical properties of high-entropy oxides (HEOs) from 2015 to 2024 was conducted, as summarized in Supplementary Table S1. The commonly utilized synthesis methods for HEO thin films and coatings include sputtering deposition, chemical vapor deposition, laser cladding, plasma spraying, pulsed laser deposition, anodizing, and the sol-gel technique, as shown in Figures 1A–G. While these techniques are well-established, the unique challenge lies in precisely controlling the HEO structure through composition and deposition parameters. For instance, in sputtering and laser deposition, differentiating HEOs from traditional oxides involves controlling composition through target composition and parameters like deposition rate, substrate temperature, and chamber pressure. Optimizing these parameters remains a significant technical barrier in HEO processing. For example, Guo et al. (2022) found that controlling the deposition rate affects both the thickness and stoichiometry of the HEO film, while variations in substrate temperature can influence crystallinity and grain size (Ling et al., 2015; Abed et al., 2024).

The common crystal structures reported for HEOs include cubic (rock-salt, fluorite), orthorhombic/tetragonal (perovskite, rutile), and their derivatives (pyrochlore, bixbyite, spinel), as illustrated in Figure 1H. The subsequent sections delve into how process parameters influence HEO formation, with a focus on crystal structure, and how crystal structure and lattice distortion impact crucial mechanical properties like hardness and elastic modulus. While limited research exists on other properties like ductility and toughness, these aspects will be revisited in the concluding summary and outlook.

3 Effects of processing parameters on HEO crystal structures

Various thin film and coating synthesis techniques have been employed for HEO production, each presenting unique challenges in controlling stoichiometry, phase formation, and microstructure due to the multi-cation nature of HEOs.

3.1 Physical and chemical vapor deposition

Physical vapor deposition (PVD) is recognized as a flexible and reliable technique for producing thin HEO films via ion bombardment (Chen and Wong, 2007; Kirnbauer et al., 2019; Yang et al., 2019; Bi et al., 2020; Khan et al., 2021; Zenkin et al.,

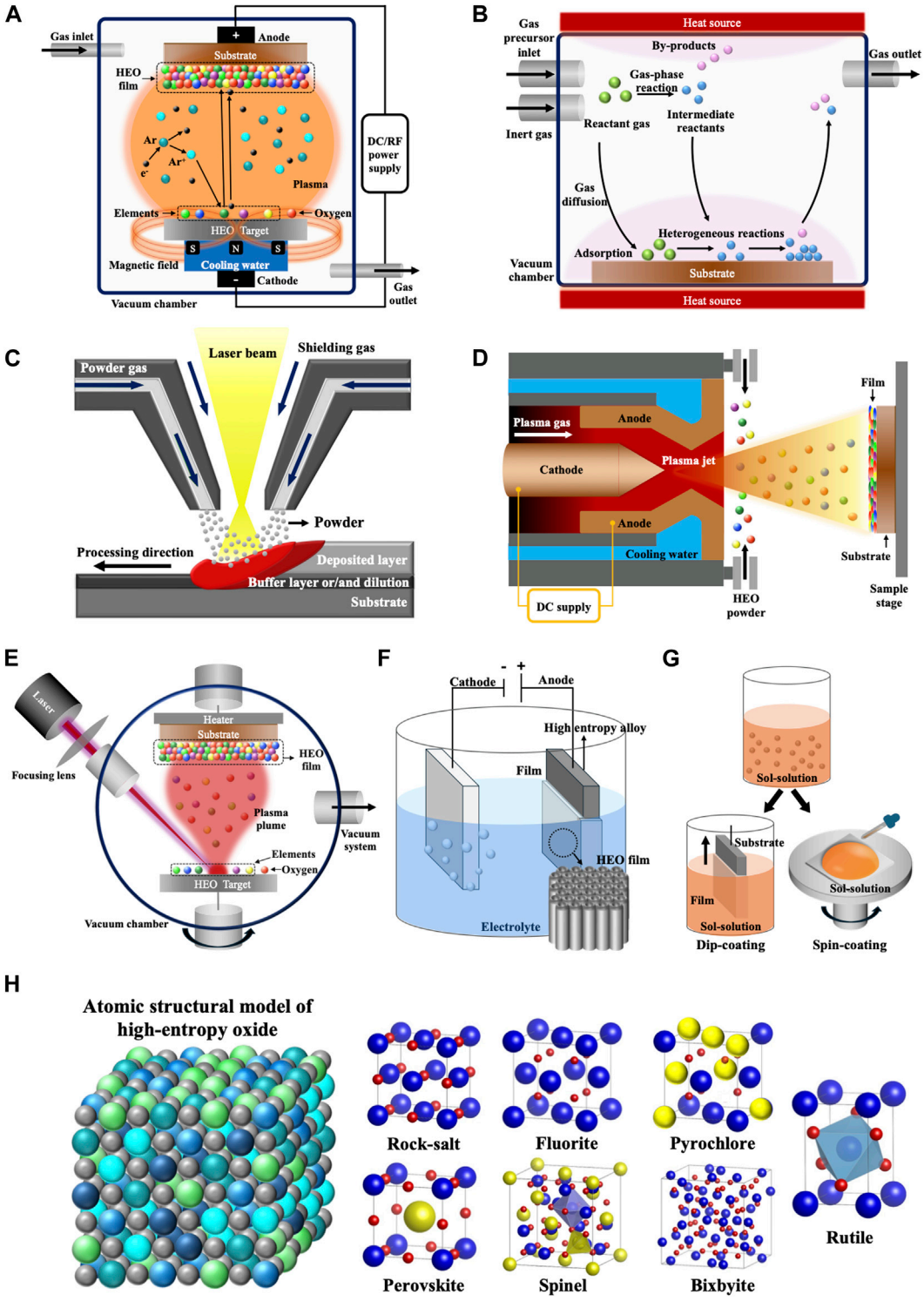

FIGURE 1
Synthesis methods for HEOs; **(A)** sputtering deposition process, **(B)** chemical vapor deposition process, **(C)** laser cladding process, **(D)** plasma spraying process, **(E)** pulsed laser deposition, **(F)** anodizing process, **(G)** sol-gel method, and **(H)** The concept and schematic structure of HEOs. The left image presents atomic structure models of a rock-salt HEO, where the metal cations of different colors are randomly distributed within an ordered crystalline lattice. The right images show the crystal structures of HEOs; anions are represented as red spheres, and cations are randomly distributed in the sublattice sites colored blue and yellow.

2023). The substrate is placed inside a high-vacuum chamber filled with an inert gas like argon, and oxygen is introduced to facilitate chemical reactions that deposit HEO films ranging from a few angstroms to several microns (Figure 1A). The deposition rate and properties of the film depend on various processing parameters including the total and partial oxygen pressures, power, voltage biases, substrate temperature, the sputtering yield, and the distance from target (Chen and Wong, 2007; Lin et al., 2010; Kirnbauer et al., 2019; Behravan et al., 2021; Salian and Mandal, 2022). For example, adjusting the oxygen partial pressure enables control of the HEO film properties, such as composition, structure, and thickness. Typically, an increase in oxygen partial pressure leads to finer and denser HEO films, enhancing their mechanical properties, while also resulting in thinner films. (Chen and Wong, 2007; Kirnbauer et al., 2019; Bi et al., 2020; Khan et al., 2021). Kirnbauer et al. (2019) found higher oxygen flow rates led to denser microstructures in (Al,Cr,Nb,Ta,Ti)O_2 films, resulting in increased hardness and elastic modulus. Meanwhile, the thickness of the (AlCrNbTaTi)O_2 film decreased from 2.7 μm to 1.6 μm as the oxygen flow ratio increased from 30% to 80%, due to a higher poisoning-state of the target. Similarly, Lin et al. (2010) observed that the thickness of a deposited (AlCrTaTiZr)O_x film reduced from 1.5 μm to 300 nm as the oxygen flow ratio increased from 2.5% to 50%. However, some researchers have also reported the opposite trends, where increasing the oxygen flow-rate ratio can lead to increased film thickness (Bi et al., 2020), indicating that these effects can vary based on the specific process conditions. Khan et al. (2021) synthesized $AlCoCrCu_{0.5}FeNi$ HEO films under different oxygen flow rates, who showed that initial increases in oxygen content led to an increase in hardness due to reduced void fractions and grain sizes. Further increasing oxygen content, however, resulted in a loss of crystallinity in the spinel HEO, with a decrease in hardness. In addition to PVD, chemical vapor deposition (CVD) method has also been demonstrated to form high-quality conformal HEO films, such as (MgCoNiCuZn)O (Raison et al., 2023), through chemical reactions of vaporized precursors on heated substrates (Figure 1B). The cation distribution remains homogeneous, matching compositions from solid-state or sputtering methods. Generally, the microstructure and properties of CVD deposited films are highly sensitive to parameters including temperature, pressure, and gas flow rates (Sabzi et al., 2023; Saringer et al., 2023). Additionally, film thickness linearly increases withe deposition time, ranging from a few hundred nanometers up to several hundred microns (Choy, 2003).

3.2 Laser-based cladding and deposition

Laser cladding has also been used to produce HEO films (Figure 1C). For example, Zhang et al. (2023a) applied laser cladding to $(LaNdSmEuGd)_2Zr_2O_7$ powders onto a NiCoCrAlY substrate that was coated with Y_2O_3-stabilized ZrO_2. They found that differences in thermal expansion coefficients among layers and phase transitions within the HEO can lead to the formation of cracks on the cladded surface, penetrating the HEO coating. Another related laser-based synthesis technique is pulsed laser deposition. High-power laser pulses evaporate a HEO target within a vacuum chamber, with the resulting plume being directed onto the substrate, depositing films ranging from a few nanometers to several microns in thickness (Figure 1E) (Kotsonis et al., 2018; Ahn et al., 2021; Jacobson et al., 2021). Both the deposition rate and the properties of the film depend on processing factors such as laser intensity, substrate temperature, and ambient oxygen pressure (Salian and Mandal, 2022). Kotsonis et al. (2018) found that single-phase MgNiCoCuZnScO films form under high kinetic energy (low pressure) conditions, while low kinetic energy (high pressure) leads to phase separation. A higher O_2/Ar ratio at low pressure also promotes phase separation. Jacobson et al. (2021) observed that the texture and lattice parameter of (MgCoNiCuZn)O films can be controlled through substrate temperature and oxygen partial pressure. However, the oxygen partial pressure might have little impact on film thickness; the thickness of these films remained constant at about 250 nm despite a decrease in the oxygen pressure from 100 mT to 50 mT. Conversely, when the laser pulse energy was increased by 30% from 200 mJ, the film thickness increased from approximately 250–470 nm.

3.3 Thermal plasma spraying

Thermal plasma spraying melts and deposits HEO particles onto substrates in a cost-effective manner (Figure 1D). During plasma spraying, fine HEO particles are melted in a thermal plasma jet and sprayed onto a substrate, forming layers of lamellae or splats upon solidification (Zhou et al., 2020; Park et al., 2021; Wang et al., 2022; Chen Z. et al., 2023). Typically, the coatings are deposited with thicknesses ranging from several tens to hundreds of micrometers but can reach up to a few millimeters. Zhou et al. (2020) utilized atmospheric plasma spraying with $(LaNdSmEuGd)_2Zr_2O_7$ powder on a superalloy substrate and deposited a coating approximately 200 μm thick that was tightly bonded and free of large pores. They observed compositional variations in the coating due to varying volatility of oxides during the process. On the other hand, Chen Z. et al. (2023) deposited $(YbYLuHoEr)_2Si_2O_7$ with a thickness of about 100 μm and found that the elements losses in $(YbYLuHoEr)_2Si_2O_7$ due to volatilization were similar across different oxides, despite varying saturated vapor pressures, suggesting that the effect of varied saturated vapor pressure on coating quality is limited. In addition to these compositional changes, process parameters significantly influence coating properties (Swain et al., 2018). Generally, reduced porosity and enhanced hardness are achieved with a finer particle size and higher substrate temperature. Meanwhile, increased spraying current and plasma power directly result in thicker coatings (Verbeek, 1992).

3.4 Electrochemical anodization

Electrochemical anodization produces self-assembled amorphous HEO nanotube arrays with a thickness of tens of microns on high-entropy alloy precursors (Figure 1F) (Makurat-Kasprolewicz and Ossowska, 2023). For example, Lei et al. (2018) employed anodic oxidation on TaNbHfZrTi high-entropy alloy to synthesize (Ta,Nb,Hf,Zr,Ti)O nanotube arrays. The anodization voltage and fluoride concentration have a linear relationship with the thickness of the nanotubes (Shi et al., 2022). However, excessive

voltage and fluoride exposure can lead to thinner layers due to electro-polishing or chemical etching (Shi et al., 2022).

3.5 Sol-gel method

The sol-gel method produces HEO coatings at low temperatures in a cost-effective manner, encompassing both dip- and spin-coating processes (Figure 1G). Einert et al. (2023) utilized dip-coating to form an amorphous HEO, which then crystallized into nanocrystalline (CoNiCuZnMg)Fe_2O_4 upon subsequent annealing. They observed that the thickness of the HEO film increased from 190 nm to 330 nm when the withdrawal speed was doubled from 8 mm/s to 16 mm/s (Einert et al., 2023), reflecting the parabolic increase in film thickness with faster substrate speeds in the draining region (high speed region) (Chen R. et al., 2023). This higher speed resulted in a thicker film with less homogeneous morphologies and more structural defects (Einert et al., 2023). Besides withdrawal speed, fluid properties such as surface tension, viscosity, and density significantly affect both the thickness and quality of the coating in dip-coating processes (Brinker et al., 1991; Fernández-Hernán et al., 2021). Post-heat treatment parameters, including annealing temperature and duration, should also be considered. Wu et al. (2024) synthesized a nanocrystalline CoNiFeCrMnO_x thin film through dip-coating. At lower post-annealing temperatures, the films showed a tendency towards particle agglomeration, whereas at higher temperatures, the formation of mesoporous HEO films was more pronounced. Einert et al. (2023) found that the thickness of nanocrystalline (CoNiCuZnMg)Fe_2O_4 increased from 190 nm to 230 nm as the post-annealing time was extended from 10 min to 2 h.

Spin coating processes are also used for various HEO applications, including semiconductors and electrocatalysts. The spin-coated film properties are primarily determined by two independent process parameters—fluid flow, which is governed by spin speed and viscosity, and the rate of evaporation (Sahu et al., 2009). Baek et al. (2023) spin-coated a spinel HEO film approximately 50 nm thick, comprising Co, Fe, Ni, Cr, and Mn, on fluorine-doped tin oxide glass substrates. The process was performed at 3,000 rpm for 20 s, repeated twice, followed by flame annealing at 1,000°C for 30 s. Ma (2023) fabricated spinel MnCoNiXYO_4 (X, Y = Mg, Cu, Zn) films on Si substrates by spin coating at 3,000 rpm for 30 s, repeated eight times, followed by a subsequent heat treatment at 750°C for 1 h. Huang and Chang (2021) synthesized amorphous (AlTiVZrHf)O_x films approximately 15 nm thick on (100) Si substrates using spin coating at 3,500 rpm for 60 s, followed by annealing at 400°C for 1 h. They enhanced adhesion to substrates and minimized defect formation by adjusting the viscosity of the precursor solutions through the types and amounts of solvents used, as well as by optimizing annealing conditions such as temperature, pressure, and duration.

3.6 Other manufacturing methods

High-temperature oxidation of sputtered high-entropy alloy films yields dense, layered HEO coatings driven by thermodynamics and cation diffusivities (Minouei et al., 2022). For example, Minouei et al. (2022) showed that oxidation of CoCrFeMnNi high-entropy alloy at 850°C for 30 min in an atmosphere of 20% O2/Ar ratio results in a spinel $(CrMnFeCoNi)_3O_4$ HEO film, approximately 510 nm thick. However, during oxidation, the inner and outer layers often exhibit distinct compositions and microstructures. Li et al. (2024) developed $AlTiVCrNi_5$ and oxidized it at 1,000°C to form a complex concentrated oxide. This process yielded a multi-layered structure, featuring a dense NiO outer layer, an intermediate layer of medium entropy oxides, and HEOs with a nano-NiO internal layer. While limited work exists, additive manufacturing techniques like 3D extrusion combined with pressureless sintering have enabled fabrication of bulk HEO ceramics. For example, Chen R. et al. (2023) were the first to utilize a 3D extrusion technique, employing oxide precursors and pressureless sintering, to produce $(MgCoNiCuZn)_{0.7}Li_{0.3}O$. The HEOs achieved a relative density of 92% when using ink with a solid content of 78 wt%, after undergoing pressureless sintering at 800°C.

Overall, precise control over HEO stoichiometry, phase, and microstructure remains challenging due to the intricate interplay between deposition/synthesis parameters and multi-cation compositions. Optimizing these techniques is crucial for realizing desired structures and properties in HEO thin films and coatings.

4 Effects of crystal structure on mechanical properties

This section delves into the mechanical properties and deformation mechanisms of the HEO family, highlighting the role of various cation elements within HEOs. Particularly, the effect of lattice distortion (δ) on mechanical properties is discussed, which is calculated according to Eq. 1 (Wright et al., 2020a):

$$\delta = \sqrt{\sum c_i \left(1 - r_i/\bar{r}\right)^2}, \quad (1)$$

where c_i, r_i and $\bar{r}$ are the atomic fraction, the radius of the i^{th} component, and average radius of multiple cations, respectively. The equation is modified for the fluorite, pyrochlore, and perovskite, which feature A-site and B-site sublattices, as shown in Eq. 2 (Wright et al., 2020a):

$$\delta = \sqrt{\delta_A^2 + \delta_B^2} \quad (2)$$

Figures 2A, B summarizes the hardness (H), elastic modulus (E), and H/E ratio as a function of HEOs crystal structures using data detailed in Supplementary Table S1. First of all, the data show that H tend to increase with E, regardless of crystal structure and composition of the HEO. This trend is in good agreement with prior first-principles calculation results (Chong et al., 2017). In terms of the effects of crystal structures, rutile structure exhibits the highest hardness and elastic modulus among all the HEO structures. Fluorite generally shows greater hardness than pyrochlore, a difference likely stemming from inherent structural differences (Chong et al., 2017; Karthick et al., 2021; Liu et al., 2022). Typically, HEOs composed of elements with smaller ionic radius and stronger bonds exhibit higher hardness (Song et al., 2021; Liew et al., 2022; Sang et al., 2023). However, for nearly identical compositions, the impact of cation radius on hardness appears minimal (Karthick et al., 2021). The greater structural order in fluorite compared to pyrochlore might account for its higher hardness (Chong et al., 2017; Karthick et al., 2021; Liu et al., 2022).

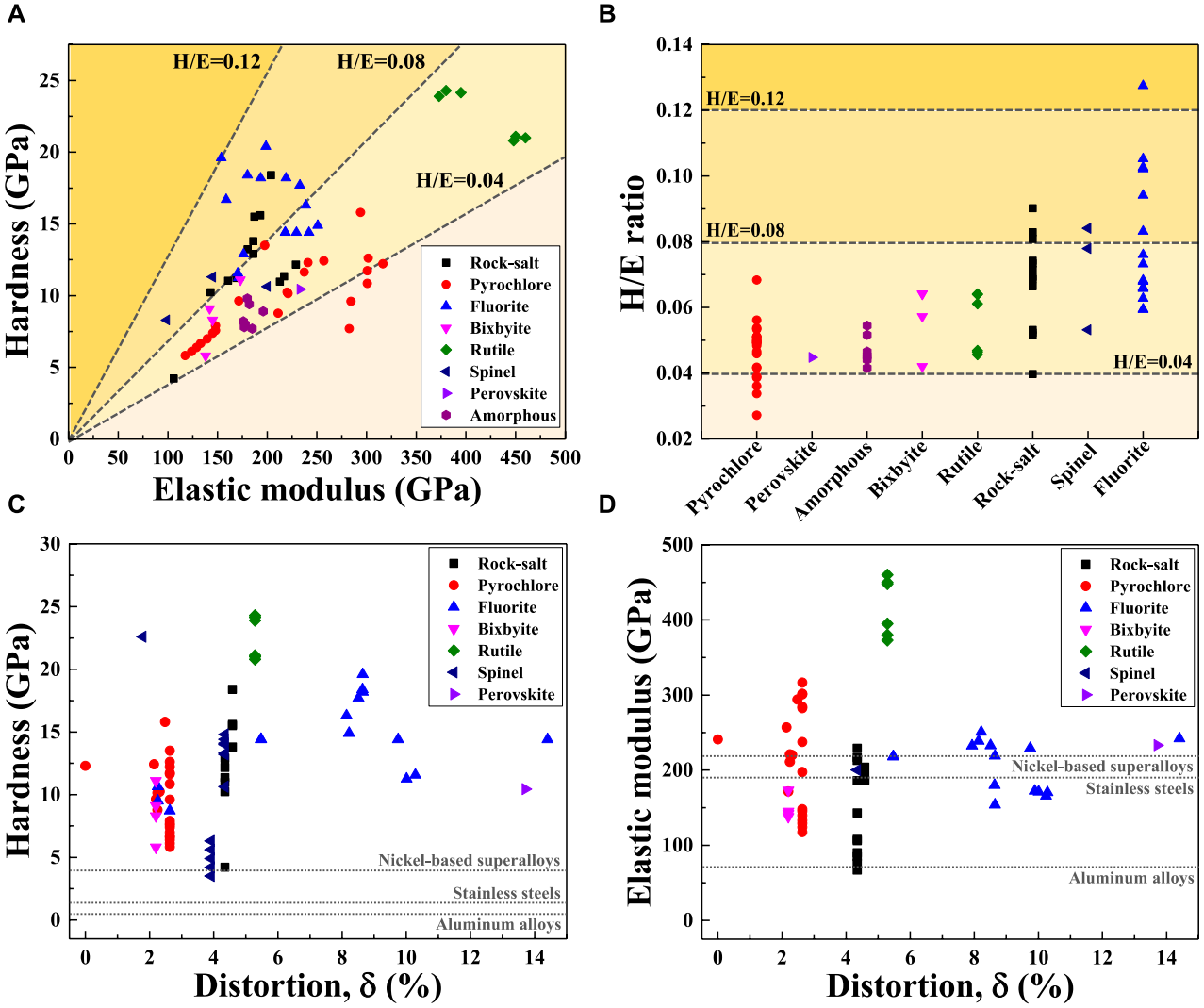

FIGURE 2
Summary of mechanical properties of HEOs from a literature survey; **(A)** elastic modulus and hardness, **(B)** H/E ratio, **(C)** hardness, and **(D)** elastic modulus with distortion across different HEO structures. The hardness and elastic modulus of several important engineering metals are also included for comparison, which are common substrate materials for such coatings.

H/E ratio is often used as an indicator of wear resistance, with a higher H/E ratio generally indicating better wear resistance of coatings (Leyland and Matthews, 2000). The H/E ratios in most HEO structures fall within 0.04–0.08, as indicated by the dashed lines in Figures 2A, B. Fluorite exhibits the higher H/E ratio (between 0.08 and 0.12) among all structures, thus likely showing great wear resistance. However, it should be noted that ranking a clear hierarchy among the mechanical properties of HEO structures is challenging due to the multitude of factors influencing their performance, such as composition, density, and grain size. This phenomenon is particularly evident in HEOs used as coatings or films. Even when deposited with identical compositions under the same process parameters, coatings of varying thicknesses can exhibit different mechanical properties due to intrinsic microstructural variations, their interaction with the substrate, and the thickness itself (Chen et al., 2005). First of all, coatings or films often exhibit microstructural inhomogeneity across their thickness due to varying grain growth mechanisms. For instance, a PVD-deposited film shows larger grain sizes on the outmost surface and smaller grains underneath, inducing variations in mechanical properties across the thickness (Bouzakis et al., 2004). Dudnik et al. (2021) physically vapor-deposited high-entropy multicomponent zirconate films with thicknesses of 70 μm and 85 μm. They found that the 85 μm film exhibited higher overall microhardness of 6,110 MPa, 3,675 MPa, and 2,860 MPa at the bottom, middle, and top, respectively, compared to the relatively lower values of 2,696 MPa, 2,273 MPa, and 1,354 MPa in the 70 μm film. These variations across thickness and differences in microhardness are attributed to compositional changes in Ce, La, Nd, and Zr, which are caused by differing evaporation behaviors during the process, as well as potentially by variations in the microlayer thickness development.

Second, in a film/substrate composite system, the thickness of the film directly determines the influence of the substrate, consequently affecting the composite's hardness and elastic modulus (Chen et al., 2005). Bi et al. (2020) found that a sputtered $(NbMoTaWV)_{78.46}O_{21.54}$

film with a thickness of 603 nm exhibited stable hardness and elastic modulus, even when the indentation depth reached 300 nm, which is 50% of the film thickness. However, Gopalan et al. (2022) found that the elastic modulus of a 3 μm thick sputtered high entropy ceramic film continuously decreased with increasing indentation depths ranging from 100 nm to 300 nm, which correspond to 3%–10% of the thickness, due to the increased contribution from the elastically compliant Si substrate. Similarly, Xing et al. (2018) found that the hardness of a sputtered high entropy ceramic film was influenced by the substrate when the indenter displacement exceeded 40% of the film thickness. Lastly, from a processing perspective, the thickness itself can influence the mechanical properties. Peng et al. (2013) found that the maximum bonding strength of a thermally sprayed coating with a thickness of 240 μm was approximately 41 MPa, which rapidly decreased to 25 MPa when the coating thickness increased to 750 μm. This reduced bonding strength in thicker coatings was attributed to high residual stress, resulting from a mismatch in thermal expansion between the coating and substrate, as well as the rapid cooling rate of the coating.

In high entropy materials, lattice distortion induced by size disorder is thought to enhance mechanical properties through solid solution strengthening (Oses et al., 2020; Wang et al., 2023; Zhang et al., 2024). On one hand, lattice distortion can impede dislocation movement (Song et al., 2021). On the other hand, a solid solution containing cations with a smaller ionic radius and greater ionic charge leads to stronger bonds, thereby enhancing mechanical properties such as elastic modulus (Wu et al., 2020; Song et al., 2021; Liew et al., 2022; Sang et al., 2023). This concept has also been well-established in high entropy alloys (Roy et al., 2021; Tandoc et al., 2023). However, the relationship between lattice distortion and mechanical properties in HEOs turned out to be complex and multifaceted. As illustrated in Figures 2C, D, δ varies according to the HEO structure type, which does not always result in predictable changes in mechanical properties; an increase in δ within a given structure can sometimes lead to reduced properties (such as hardness for fluorite). This indicates the influence of other factors beyond lattice disorder on mechanical properties. Particularly, grain size, density, and porosity need to be considered alongside lattice distortion, as smaller grain sizes, higher densities, and uniformly distributed pores generally enhance hardness (Hong et al., 2019; Mao et al., 2021; Guo et al., 2023; Zhang et al., 2024). Indeed, several recent reports show that lattice distortion does not invariably benefit mechanical properties of HEOs. For example, Zhao (2021) found that lattice distortion can soften the elastic modulus by promoting electronic charge delocalization. Similarly, Sharma and Balasubramanian (2023) identified that bond lengthening and angular distortions could lead to a decrease in the elastic modulus.

5 Mechanical behavior of HEOs under extreme temperatures and pressures

Typically, with increasing temperature, HEOs demonstrate a tendency towards softening, with reduced elastic modulus, shear modulus, and hardness (Ren et al., 2019; Rost et al., 2022; Fu et al., 2024). This effect is likely due to increased atomic thermal motion at higher temperatures, leading to expanded interatomic spacing and weakened atomic forces, thus reducing the stiffness (Li et al., 2011). Fu et al. (2024) demonstrated that both the elastic modulus and shear modulus of $(LaYSmEuGd)_2Zr_2O_7$ decrease with increasing temperature from room temperature to 1,200°C, with the elastic modulus from 148 GPa to 117 GPa, and the shear modulus from 57 GPa to 45 GPa. It should also be considered that phase transformations of HEOs can occur at high temperatures. Rost et al. (2022) measured the hardness and elastic modulus of (MgNiCoCuZn)O while thermally cycling it from room temperature to 950°C three times. The hardness and elastic modulus significantly softened as the temperature increased to 850°C, dropping from 4 GPa to 1.5 GPa and from 110 GPa to 40 GPa, respectively. Upon further heating, the HEO phase transformed, resulting in a stepwise increase in the elastic modulus to 65 GPa, but hardness did not increase and continue to soften. Throughout the heating cycles, the properties were reversible and dependent solely on temperature, showing no degradation with repeated cycles. It might be more challenging to predict temperature-dependent properties, especially in the HEO system. Ren et al. (2019) found that the elastic modulus of $(YHoErYb)_2SiO_5$ at 1,300°C is 8% higher than predicted by the mixture rule, attributed to the cocktail effect. As a result, $(YHoErYb)_2SiO_5$ demonstrates remarkable retention of high-temperature elastic stiffness, with only an 11% decrease from 170 GPa to 150 GPa. Additionally, a change to a preferred orientation at high temperatures can also significantly affect high-temperature mechanical properties. Kirnbauer et al. (2019) exhibited that as the random orientation of rutile (Al,Cr,Nb,Ta,Ti)O_2 developed into a highly (Guo et al., 2023) textured orientation after annealing above 1,000°C, the hardness decreased from 24 GPa to 21 GPa and the elastic modulus increased from 400 GPa to 460 GPa.

In addition to temperature, pressure is also found to significantly influence the deformation mechanisms and phase transformations in HEOs (Cheng et al., 2019; Yue et al., 2022). Yue et al. (2022) observed a transition from anisotropy to isotropy in (Co,Cu,Mg,Ni,Zn)O at pressures above 20 GPa, with this structural evolution altering the slip system from $<011>\{100\}$ to $<1\bar{1}0>\{110\}$. This change aligns with that compression over 20 GPa suppresses the Jahn–Teller effect in CuO_6 octahedra, causing the distorted lattice to become nearly cubic (Yan et al., 2021), thereby reducing the Jahn–Teller effect that facilitates deformation in (Mg,Co,Ni,Cu,Zn)O (Wang et al., 2023). Furthermore, high pressure can break down the long-range lattice connectivity and lead to amorphization, potentially eliminating the dislocation slip system, as demonstrated in $(CeLaPrSmY)O_{2-\delta}$ HEO system (Cheng et al., 2019).

HEOs are primarily utilized as coatings or films (rather than as structural materials) to protect the substrates from the extreme environments, with their application as thermal barrier coatings being a prime example. Hence, understanding how coating characteristics, such as thickness and microstructural variations across the depth, especially in high temperatures, influence the coating performance is crucial. Dudnik et al. (2021) found that increasing HEO coating thickness from 70 μm to 85 μm increased the hardness. Similar effects are also observed at high temperature, where Wu et al. (2023) showed that thicker thermal barrier coatings led to increased hardness and elastic modulus at the surface due to greater sintering facilitated by higher surface temperatures. This, in turn, negatively impacts thermal cycling performance due to

increased thermal stress caused by larger differences in elastic modulus. Typically, thinner coatings have higher fracture toughness, and exhibit better resistance to thermal stress-induced failures. Lu et al. (2019) showed that increasing the coating thickness resulted in a significant compressive stress gradient and increased strain energy, which increased the hardness and elastic modulus at the interface, reducing fracture toughness and thereby diminishing the thermal shock resistance. Similarly, Zhang et al. (2023a), Zhang et al. (2023b) observed that thinner laser-cladded double-layer coatings, comprising a pyrochlore structure HEO and an yttria-stabilized zirconia buffer layer on a NiCoCrAlY alloy substrate, exhibit higher thermal cycling resistance. Specifically, debonding at the interface between the buffer layer and the substrate occurred after 40 cycles at 1,050°C for coatings with thicknesses of 305 μm. In contrast, for coatings of 264 μm, debonding occurred after 70 cycles.

Furthermore, thickness is a critical factor in determining the failure behavior of coatings induced by thermal stress. For example, Wu et al. (2023) demonstrated how coating thickness influences the temperature and its distribution within the coating, thereby affecting microstructure evolution, the thickness of thermally grown oxides, and sintering behaviors. They found that in relatively thin 100 μm air-plasma-sprayed coatings, the stress from thermally grown oxides, induced by intensive oxidation, dominates the failure behavior. In contrast, in thicker coatings of 400 μm, sintering behavior becomes predominant, causing failure by increasing the modulus at the surface, which experiences higher temperatures.

6 Summary and outlook

HEOs represent a promising class of ceramic materials with tunable compositions and mechanical properties, making them attractive candidates for future high-temperature applications. This review elucidates the critical interplay between processing methods, resulting crystal structures, and mechanical behavior of HEOs under extreme environments. The synthesis processes for HEO thin films and coatings play a pivotal role in determining their compositions, crystallinity, phase formations, defect densities, and thickness, which directly influence their mechanical properties. Among the various crystal structures exhibited by HEOs, rutile-structured compositions have demonstrated superior elastic modulus and hardness, and fluorite-structured compositions exhibited the highest tendency for wear resistance compared to other structures. Interestingly, while lattice distortion was initially considered a reliable predictor of mechanical properties in high-entropy materials, it does not consistently correlate with the observed changes in HEOs.

For high-temperature applications, a comprehensive understanding of the temperature-dependent mechanical behavior of HEOs is imperative. Notably, there is a lack of experimental data on the plastic deformation and strain tolerance of HEOs both in bulk and as films in the current literature. Additionally, more experimental measurements of temperature-dependent dislocation behavior are needed, as these factors are crucial determinants of creep and high temperatures mechanical properties. High-throughput synthesis techniques capable of rapidly exploring a larger compositional space, including stoichiometric and off-stoichiometric HEO compositions, are highly desirable to accelerate the development of mechanically robust HEOs. Furthermore, the development of multiphase structures and precipitates in HEOs beyond single-phase solid solutions presents an opportunity to further enhance their mechanical properties.

Overall, this review underscores the immense potential of HEOs as promising high-temperature materials and emphasizes the need for a comprehensive understanding of their processing-structure-property relationships, temperature-dependent behavior, and computationally-guided design approaches to unlock their full potential in extreme environments.

Author contributions

JL: Conceptualization, Data curation, Formal Analysis, Investigation, Methodology, Validation, Visualization, Writing–original draft. WC: Conceptualization, Funding acquisition, Project administration, Supervision, Writing–review and editing.

Funding

The author(s) declare that financial support was received for the research, authorship, and/or publication of this article. Funding is provided by US National Science Foundation (DMR-2104655/2104656) and Virginia Tech.

Acknowledgments

The authors gratefully acknowledge funding provided by US National Science Foundation (DMR- 2104655/2104656) and Virginia Tech.

Conflict of interest

The authors declare that the research was conducted in the absence of any commercial or financial relationships that could be construed as a potential conflict of interest.

The author(s) declared that they were an editorial board member of Frontiers, at the time of submission. This had no impact on the peer review process and the final decision.

Publisher's note

Supplementary material

The Supplementary Material for this article can be found online at: https://www.frontiersin.org/articles/10.3389/frcdi.2024.1417527/full#supplementary-material

References

Abed, N. Z., Ismail, R. A., and Shaker, S. S. (2024). Role of substrate temperature on the performance of BaTiO3/Si photodetector prepared by pulsed laser deposition. *Sci. Rep.* 14 (1), 4531. doi:10.1038/s41598-024-55053-1

Ahn, M., Park, Y., Lee, S. H., Chae, S., Lee, J., Heron, J. T., et al. (2021). Memristors based on (Zr, Hf, Nb, Ta, Mo, W) high-entropy oxides. *Adv. Electron. Mater.* 7 (5), 2001258. doi:10.1002/aelm.202001258

Akrami, S., Edalati, P., Fuji, M., and Edalati, K. (2021). High-entropy ceramics: review of principles, production and applications. *Mater. Sci. Eng. R Rep.* 146, 100644. doi:10.1016/j.mser.2021.100644

Albedwawi, S. H., AlJaberi, A., Haidemenopoulos, G. N., and Polychronopoulou, K. (2021). High entropy oxides-exploring a paradigm of promising catalysts: a review. *Mater. Des.* 202, 109534. doi:10.1016/j.matdes.2021.109534

Baek, J., Hossain, M. D., Mukherjee, P., Lee, J., Winther, K. T., Leem, J., et al. (2023). Synergistic effects of mixing and strain in high entropy spinel oxides for oxygen evolution reaction. *Nat. Commun.* 14 (1), 5936. doi:10.1038/s41467-023-41359-7

Behravan, N., Farhadizadeh, A., Ghasemi, S., Khademi, A., Shojaei, H., and Ghomi, H. (2021). The pressure dependence of structure and composition of sputtered AlCrSiTiMoO high entropy thin film. *J. Alloys Compd.* 852, 156421. doi:10.1016/j.jallcom.2020.156421

Bérardan, D., Franger, S., Dragoe, D., Meena, A. K., and Dragoe, N. (2016). Colossal dielectric constant in high-entropy oxides. *Phys. status solidi (RRL)–Rapid Res. Lett.* 10 (4), 328–333. doi:10.1002/pssr.201600043

Bi, L., Li, X., Li, Z., Hu, Y., Zhang, J., Wang, Q., et al. (2020). Performance and local structure evolution of NbMoTaWV entropy-stabilized oxide thin films with variable oxygen content. *Surf. Coatings Technol.* 402, 126326. doi:10.1016/j.surfcoat.2020.126326

Bouzakis, K. D., Hadjiyiannis, S., Skordaris, G., Mirisidis, I., Michailidis, N., Efstathiou, K., et al. (2004). The effect of coating thickness, mechanical strength and hardness properties on the milling performance of PVD coated cemented carbides inserts. *Surf. Coatings Technol.* 177-178, 657–664. doi:10.1016/j.surfcoat.2003.08.003

Braun, J. L., Rost, C. M., Lim, M., Giri, A., Olson, D. H., Kotsonis, G. N., et al. (2018). Charge-induced disorder controls the thermal conductivity of entropy-stabilized oxides. *Adv. Mater.* 30 (51), 1805004. doi:10.1002/adma.201805004

Brinker, C. J., Frye, G. C., Hurd, A. J., and Ashley, C. S. (1991). Fundamentals of sol-gel dip coating. *Thin Solid Films* 201 (1), 97–108. doi:10.1016/0040-6090(91)90158-t

Chen, J., Liu, W. X., Liu, J. X., Zhang, X. L., Yuan, M. Z., Zhao, Y. L., et al. (2019). Stability and compressibility of cation-doped high-entropy oxide MgCoNiCuZnO5. *J. Phys. Chem. C* 123 (29), 17735–17744. doi:10.1021/acs.jpcc.9b04992

Chen, K., Pei, X., Tang, L., Cheng, H., Li, Z., Li, C., et al. (2018). A five-component entropy-stabilized fluorite oxide. *J. Eur. Ceram. Soc.* 38 (11), 4161–4164. doi:10.1016/j.jeurceramsoc.2018.04.063

Chen, R., Li, S., Yan, Q., and Wen, H. (2023b). Additive manufacturing of (MgCoNiCuZn)O high-entropy oxide using a 3D extrusion technique and oxide precursors. *Ceram. Int.* 49 (20), 33432–33436. doi:10.1016/j.ceramint.2023.08.061

Chen, S., Liu, L., and Wang, T. (2005). Investigation of the mechanical properties of thin films by nanoindentation, considering the effects of thickness and different coating–substrate combinations. *Surf. Coatings Technol.* 191 (1), 25–32. doi:10.1016/j.surfcoat.2004.03.037

Chen, T.-K., and Wong, M.-S. (2007). Structure and properties of reactively-sputtered AlxCoCrCuFeNi oxide films. *Thin Solid Films* 516 (2-4), 141–146. doi:10.1016/j.tsf.2007.06.142

Chen, Z., Lin, C., Zheng, W., Jiang, C., Song, X., and Zeng, Y. (2023a). A high-entropy (Yb0.2Y0.2Lu0.2Ho0.2Er0.2)2Si2O7 environmental barrier coating prepared by atmospheric plasma-spray. *Ceram. Int.* 49 (7), 11323–11333. doi:10.1016/j.ceramint.2022.11.332

Cheng, B., Lou, H., Sarkar, A., Zeng, Z., Zhang, F., Chen, X., et al. (2020). Lattice distortion and stability of (Co0.2Cu0.2Mg0.2Ni0.2Zn0.2)O high-entropy oxide under high pressure. *Mater. Today Adv.* 8, 100102. doi:10.1016/j.mtadv.2020.100102

Cheng, B., Lou, H., Sarkar, A., Zeng, Z., Zhang, F., Chen, X., et al. (2019). Pressure-induced tuning of lattice distortion in a high-entropy oxide. *Commun. Chem.* 2 (1), 114. doi:10.1038/s42004-019-0216-2

Chong, X., Jiang, Y., Hu, M., and Feng, J. (2017). Elaborating the phases and mechanical properties of multiphase alloy: experimental two-dimensional mapping combined with theoretical calculations. *Mater. Charact.* 134, 347–353. doi:10.1016/j.matchar.2017.11.005

Choy, K. L. (2003). Chemical vapour deposition of coatings. *Prog. Mater. Sci.* 48 (2), 57–170. doi:10.1016/s0079-6425(01)00009-3

Dong, Y., Ren, K., Lu, Y., Wang, Q., Liu, J., and Wang, Y. (2019). High-entropy environmental barrier coating for the ceramic matrix composites. *J. Eur. Ceram. Soc.* 39 (7), 2574–2579. doi:10.1016/j.jeurceramsoc.2019.02.022

Dudnik, O., Lakiza, S., Grechanyuk, I., Red'ko, V., Glabay, M., Shmibelsky, V., et al. (2021). High-entropy ceramics for thermal barrier coatings produced from ZrO 2 doped with rare-earth metal oxides. *Powder Metallurgy Metal Ceram.* 59, 556–563. doi:10.1007/s11106-021-00187-4

Dupuy, A. D., Wang, X., and Schoenung, J. M. (2019). Entropic phase transformation in nanocrystalline high-entropy oxides. *Mater. Res. Lett.* 7 (2), 60–67. doi:10.1080/21663831.2018.1554605

Einert, M., Waheed, A., Lauterbach, S., Mellin, M., Rohnke, M., Wagner, L. Q., et al. (2023). Sol-gel-derived ordered mesoporous high entropy spinel ferrites and assessment of their photoelectrochemical and electrocatalytic water splitting performance. *Small* 19 (14), 2205412. doi:10.1002/smll.202205412

Fernández-Hernán, J. P., López, A. J., Torres, B., and Rams, J. (2021). Influence of roughness and grinding direction on the thickness and adhesion of sol-gel coatings deposited by dip-coating on AZ31 magnesium substrates. A Landau–Levich equation revision. *Surf. Coatings Technol.* 408, 126798. doi:10.1016/j.surfcoat.2020.126798

Fu, M., Ma, X., Zhao, K., Li, X., and Su, D. (2021). High-entropy materials for energy-related applications. *iScience* 24 (3), 102177. doi:10.1016/j.isci.2021.102177

Fu, S., Jia, Z., Wan, D., and Bao, Y. (2024). Synthesis, microstructure and thermophysical properties of (La0.2Y0.2Sm0.2Eu0.2Gd0.2)2Zr2O7 high-entropy oxide ceramic. *Ceram. Int.* 50 (3), 5510–5515. doi:10.1016/j.ceramint.2023.11.306

Gao, Y., Liu, Y., Yu, H., and Zou, D. (2022). High-entropy oxides for catalysis: status and perspectives. *Appl. Catal. A General* 631, 118478. doi:10.1016/j.apcata.2022.118478

Gopalan, H., Marshal, A., Hans, M., Primetzhofer, D., Cautaerts, N., Breitbach, B., et al. (2022). On the interplay between microstructure, residual stress and fracture toughness of (Hf-Nb-Ta-Zr) C multi-metal carbide hard coatings. *Mater. Des.* 224, 111323. doi:10.1016/j.matdes.2022.111323

Guo, H., Wang, X., Dupuy, A. D., Schoenung, J. M., and Bowman, W. J. (2022). Growth of nanoporous high-entropy oxide thin films by pulsed laser deposition. *J. Mater. Res.* 37, 124–135. doi:10.1557/s43578-021-00473-2

Guo, Y., Zheng, R., Feng, S., Fu, J., Yang, Y., Wang, H., et al. (2023). High-entropy (Ho0.2Y0.2Dy0.2Gd0.2Eu0.2)2Ti2O7/TiO2 composites with excellent mechanical and thermal properties. *J. Eur. Ceram. Soc.* 43 (14), 6398–6406. doi:10.1016/j.jeurceramsoc.2023.06.024

Hong, W., Chen, F., Shen, Q., Han, Y. H., Fahrenholtz, W. G., and Zhang, L. (2019). Microstructural evolution and mechanical properties of (Mg, Co, Ni, Cu, Zn) O high-entropy ceramics. *J. Am. Ceram. Soc.* 102 (4), 2228–2237. doi:10.1111/jace.16075

Huang, Z.-W., and Chang, K.-S. (2021). Spin-coating for fabrication of high-entropy high-k (AlTiVZrHf)O films on Si for advanced gate stacks. *Ceram. Int.* 47 (16), 22558–22566. doi:10.1016/j.ceramint.2021.04.267

Jacobson, V., Diercks, D., To, B., Zakutayev, A., and Brennecka, G. (2021). Thin film growth effects on electrical conductivity in entropy stabilized oxides. *J. Eur. Ceram. Soc.* 41 (4), 2617–2624. doi:10.1016/j.jeurceramsoc.2020.12.021

Karthick, G., Raman, L., and Murty, B. S. (2021). Phase evolution and mechanical properties of novel nanocrystalline Y2(TiZrHfMoV)2O7 high entropy pyrochlore. *J. Mater. Sci. Technol.* 82, 214–226. doi:10.1016/j.jmst.2020.12.025

Khan, N. A., Akhavan, B., Zheng, Z., Liu, H., Zhou, C., Zhou, H., et al. (2021). Nanostructured AlCoCrCu0.5FeNi high entropy oxide (HEO) thin films fabricated using reactive magnetron sputtering. *Appl. Surf. Sci.* 553, 149491. doi:10.1016/j.apsusc.2021.149491

Kirnbauer, A., Spadt, C., Koller, C. M., Kolozsvári, S., and Mayrhofer, P. H. (2019). High-entropy oxide thin films based on Al–Cr–Nb–Ta–Ti. *Vacuum* 168, 108850. doi:10.1016/j.vacuum.2019.108850

Kotsonis, G. N., Almishal, S. S. I., Marques dos Santos Vieira, F., Crespi, V. H., Dabo, I., Rost, C. M., et al. (2023). High-entropy oxides: harnessing crystalline disorder for emergent functionality. *J. Am. Ceram. Soc.* 106 (10), 5587–5611. doi:10.1111/jace.19252

Kotsonis, G. N., Rost, C. M., Harris, D. T., and Maria, J.-P. (2018). Epitaxial entropy-stabilized oxides: growth of chemically diverse phases via kinetic bombardment. *MRS Commun.* 8 (3), 1371–1377. doi:10.1557/mrc.2018.184

Lai, A., Du, Z., Gan, C. L., and Schuh, C. A. (2013). Shape memory and superelastic ceramics at small scales. *Science* 341 (6153), 1505–1508. doi:10.1126/science.1239745

Lei, Z., Liu, X., Li, R., Wang, H., Wu, Y., and Lu, Z. (2018). Ultrastable metal oxide nanotube arrays achieved by entropy-stabilization engineering. *Scr. Mater.* 146, 340–343. doi:10.1016/j.scriptamat.2017.12.025

Leyland, A., and Matthews, A. (2000). On the significance of the H/E ratio in wear control: a nanocomposite coating approach to optimised tribological behaviour. *Wear* 246 (1), 1–11. doi:10.1016/s0043-1648(00)00488-9

Li, M., Sun, H., Tan, X., Zhang, H., and Liu, J. (2024). A novel entropy-stabilized oxide coating thermally grown from a valve metal-based complex concentrated alloy. *Mater. Today* 74, 46–57. doi:10.1016/j.mattod.2024.02.005

Li, W., Wang, R., Li, D., and Fang, D. (2011). A model of temperature-dependent Young's modulus for ultrahigh temperature ceramics. *Phys. Res. Int.* 2011, 1–3. doi:10.1155/2011/791545

Liew, S. L., Ni, X. P., Wei, F., Tan, S. Y., Luai, M. T., Lim, P. C., et al. (2022). High-entropy fluorite oxides: atomic stabiliser effects on thermal-mechanical properties. *J. Eur. Ceram. Soc.* 42 (14), 6608–6613. doi:10.1016/j.jeurceramsoc.2022.07.026

Lin, M.-I., Tsai, M.-H., Shen, W.-J., and Yeh, J.-W. (2010). Evolution of structure and properties of multi-component (AlCrTaTiZr) Ox films. *Thin Solid Films* 518 (10), 2732–2737. doi:10.1016/j.tsf.2009.10.142

Ling, H., and Yan, M. F. (1988). Microhardness measurements on dopant modified superconducting YBa2Cu3O7 ceramics. *J. Appl. Phys.* 64 (3), 1307–1311. doi:10.1063/1.341851

Ling, L. P., Khen, H. M., Chu, T. K., Kumari, D. N., Shan, Y. S., Hoong, O. B., et al. (2015). Substrate temperature and background pressure effects on nanostructured zinc oxide thin films for thermoelectric applications. *Int. J. Nanoelectron. Mater* 8, 7–14.

Liu, D., Shi, B., Geng, L., Wang, Y., Xu, B., and Chen, Y. (2022). High-entropy rare-earth zirconate ceramics with low thermal conductivity for advanced thermal-barrier coatings. *J. Adv. Ceram.* 11 (6), 961–973. doi:10.1007/s40145-022-0589-z

Liu, X., Zhang, P., Han, Y., Pan, W., and Wan, C. (2023a). Tailoring thermal and mechanical properties of rare earth niobates by coupling entropy and composite engineering. *J. Eur. Ceram. Soc.* 43 (3), 1141–1146. doi:10.1016/j.jeurceramsoc.2022.10.081

Lu, F., Huang, W., and Liu, H. (2019). Mechanical properties and thermal shock resistance of 8YSZ-Al 2 O 3 composite coatings with different thicknesses. *J. Therm. Spray Technol.* 28, 1893–1905. doi:10.1007/s11666-019-00946-1

Ma, C. (2023). Modulation of optical absorption and electrical properties in Mn-Co-Ni-O-based high-entropy thin films. *Front. Mater.* 10, 1297318. doi:10.3389/fmats.2023.1297318

Makurat-Kasprolewicz, B., and Ossowska, A. (2023). Recent advances in electrochemically surface treated titanium and its alloys for biomedical applications: a review of anodic and plasma electrolytic oxidation methods. *Mater. Today Commun.* 34, 105425. doi:10.1016/j.mtcomm.2023.105425

Mao, H.-R., Guo, R.-F., Cao, Y., Jin, S.-B., Qiu, X.-M., and Shen, P. (2021). Ultrafast densification of high-entropy oxide (La0.2Nd0.2Sm0.2Eu0.2Gd0.2)2Zr2O7 by reactive flash sintering. *J. Eur. Ceram. Soc.* 41 (4), 2855–2860. doi:10.1016/j.jeurceramsoc.2020.11.052

Minouei, H., Kheradmandfard, M., Saboktakin Rizi, M., Jalaly, M., Kim, D.-E., and Hong, S. I. (2022). Formation mechanism of high-entropy spinel thin film and its mechanical and magnetic properties: linking high-entropy alloy to high-entropy ceramic. *Appl. Surf. Sci.* 576, 151719. doi:10.1016/j.apsusc.2021.151719

Musicó, B. L., Gilbert, D., Ward, T. Z., Page, K., George, E., Yan, J., et al. (2020). The emergent field of high-entropy oxides: design, prospects, challenges, and opportunities for tailoring material properties. *Apl. Mater.* 8 (4). doi:10.1063/5.0003149

Nallathambi, V., Bhaskar, L. K., Wang, D., Naberezhnov, A. A., Sumnikov, S. V., Ionescu, E., et al. (2023). Tuning the mechanical and thermal properties of (MgNiCoCuZn)O by intelligent control of cooling rates. *J. Eur. Ceram. Soc.* 43 (10), 4517–4529. doi:10.1016/j.jeurceramsoc.2023.03.016

Nan, H., Lv, S., Xu, Z., Feng, Y., Zhou, Y., Liu, M., et al. (2023). Inducing the cocktail effect in yolk-shell high-entropy perovskite oxides using an electronic structural design for improved electrochemical applications. *Chem. Eng. J.* 452, 139501. doi:10.1016/j.cej.2022.139501

Oses, C., Toher, C., and Curtarolo, S. (2020). High-entropy ceramics. *Nat. Rev. Mater.* 5 (4), 295–309. doi:10.1038/s41578-019-0170-8

Pang, E. L., Olson, G. B., and Schuh, C. A. (2022). Low-hysteresis shape-memory ceramics designed by multimode modelling. *Nature* 610 (7932), 491–495. doi:10.1038/s41586-022-05210-1

Park, T., Adomako, N. K., Ashong, A., Kim, Y., Yang, S., and Kim, J. (2021). Interfacial structure and physical properties of high-entropy oxide coatings prepared via atmospheric plasma spraying. *Coatings* 11 (7), 755. doi:10.3390/coatings11070755

Peng, Y., Zhang, C., Zhou, H., and Liu, L. (2013). On the bonding strength in thermally sprayed Fe-based amorphous coatings. *Surf. Coatings Technol.* 218, 17–22. doi:10.1016/j.surfcoat.2012.12.018

Raison, A., Prud'homme, N., Wang, W., Dragoe, D., and Dragoe, N. (2023). Chemical vapor deposition of entropy-stabilized rock-salt type oxide thin films. *Mater. Lett.* 337, 133955. doi:10.1016/j.matlet.2023.133955

Ren, K., Wang, Q., Shao, G., Zhao, X., and Wang, Y. (2020). Multicomponent high-entropy zirconates with comprehensive properties for advanced thermal barrier coating. *Scr. Mater.* 178, 382–386. doi:10.1016/j.scriptamat.2019.12.006

Ren, X., Tian, Z., Zhang, J., and Wang, J. (2019). Equiatomic quaternary (Y1/4Ho1/4Er1/4Yb1/4) 2SiO5 silicate: a perspective multifunctional thermal and environmental barrier coating material. *Scr. Mater.* 168, 47–50. doi:10.1016/j.scriptamat.2019.04.018

Rost, C. M., Sachet, E., Borman, T., Moballegh, A., Dickey, E. C., Hou, D., et al. (2015). Entropy-stabilized oxides. *Nat. Commun.* 6, 8485. doi:10.1038/ncomms9485

Rost, C. M., Schmuckler, D. L., Bumgardner, C., Bin Hoque, M. S., Diercks, D. R., Gaskins, J. T., et al. (2022). On the thermal and mechanical properties of Mg0. 2Co0. 2Ni0. 2Cu0. 2Zn0. 2O across the high-entropy to entropy-stabilized transition. *Apl. Mater.* 10 (12). doi:10.1063/5.0122775

Roy, A., Sreeramagiri, P., Babuska, T., Krick, B., Ray, P. K., and Balasubramanian, G. (2021). Lattice distortion as an estimator of solid solution strengthening in high-entropy alloys. *Mater. Charact.* 172, 110877. doi:10.1016/j.matchar.2021.110877

Sabzi, M., Mousavi Anijdan, S., Shamsodin, M., Farzam, M., Hojjati-Najafabadi, A., Feng, P., et al. (2023). A review on sustainable manufacturing of ceramic-based thin films by chemical vapor deposition (CVD): reactions kinetics and the deposition mechanisms. *Coatings* 13 (1), 188. doi:10.3390/coatings13010188

Sahu, N., Parija, B., and Panigrahi, S. (2009). Fundamental understanding and modeling of spin coating process: a review. *Indian J. Phys.* 83 (4), 493–502. doi:10.1007/s12648-009-0009-z

Salian, A., and Mandal, S. (2022). Review on the deposition, structure and properties of high entropy oxide films: current and future perspectives. *Bull. Mater. Sci.* 45 (1), 49. doi:10.1007/s12034-021-02617-w

Sang, W., Zhang, H., Zhang, H., Liu, X., Chen, X., Xie, W., et al. (2023). Novel (Sm0.2Lu0.2Yb0.2Y0.2Dy0.2)3TaO7 high-entropy ceramic for thermal barrier coatings. *Ceram. Int.* 49 (6), 9052–9059. doi:10.1016/j.ceramint.2022.11.061

Saringer, C., Tkadletz, M., Thurner, J., Czettl, C., and Schalk, N. (2023). Influence of deposition parameters on microstructure and mechanical properties of chemical vapor deposited Ti1-xAlxN coatings. *Int. J. Refract. Metals Hard Mater.* 113, 106203. doi:10.1016/j.ijrmhm.2023.106203

Sarkar, A., Djenadic, R., Wang, D., Hein, C., Kautenburger, R., Clemens, O., et al. (2018). Rare earth and transition metal based entropy stabilised perovskite type oxides. *J. Eur. Ceram. Soc.* 38 (5), 2318–2327. doi:10.1016/j.jeurceramsoc.2017.12.058

Sarkar, A., Wang, Q., Schiele, A., Chellali, M. R., Bhattacharya, S. S., Wang, D., et al. (2019). High-entropy oxides: fundamental aspects and electrochemical properties. *Adv. Mater.* 31 (26), 1806236. doi:10.1002/adma.201806236

Sharma, P., and Balasubramanian, G. (2023). Electronic and lattice distortions induce elastic softening in refractory multicomponent borides. *Chem. Mater.* 35 (18), 7511–7520. doi:10.1021/acs.chemmater.3c01086

Shi, Y., Li, R., and Lei, Z. (2022). Influences of synthetic parameters on morphology and growth of high entropy oxide nanotube arrays. *Coatings* 13 (1), 46. doi:10.3390/coatings13010046

Song, D., Song, T., Paik, U., Lyu, G., Jung, Y.-G., Jeon, H.-B., et al. (2021). Glass-like thermal conductivity in mass-disordered high-entropy (Y,Yb)2(Ti, Zr, Hf)2O7 for thermal barrier material. *Mater. Des.* 210, 110059. doi:10.1016/j.matdes.2021.110059

Spurling, R. J., Lass, E. A., Wang, X., and Page, K. (2022). Entropy-driven phase transitions in complex ceramic oxides. *Phys. Rev. Mater.* 6 (9), 090301. doi:10.1103/physrevmaterials.6.090301

Sun, Y., and Dai, S. (2021). High-entropy materials for catalysis: a new frontier. *Sci. Adv.* 7 (20), eabg1600. doi:10.1126/sciadv.abg1600

Swain, B. K., Mohapatra, S. S., Pattanaik, A., Samal, S. K., Bhuyan, S. K., Barik, K., et al. (2018). Sensitivity of process parameters in atmospheric plasma spray coating. *J. Therm. Spray Eng.* 1 (1), 1–6. doi:10.52687/2582-1474/111

Tandoc, C., Hu, Y.-J., Qi, L., and Liaw, P. K. (2023). Mining of lattice distortion, strength, and intrinsic ductility of refractory high entropy alloys. *npj Comput. Mater.* 9 (1), 53. doi:10.1038/s41524-023-00993-x

Toher, C., Oses, C., Hicks, D., and Curtarolo, S. (2019). Unavoidable disorder and entropy in multi-component systems. *npj Comput. Mater.* 5 (1), 69. doi:10.1038/s41524-019-0206-z

Usharani, N. J., Bhandarkar, A., Subramanian, S., and Bhattacharya, S. S. (2020). Antiferromagnetism in a nanocrystalline high entropy oxide (Co,Cu,Mg,Ni,Zn)O: magnetic constituents and surface anisotropy leading to lattice distortion. *Acta Mater.* 200, 526–536. doi:10.1016/j.actamat.2020.09.034

Verbeek, A. T. J. (1992). Plasma sprayed thermal barrier coatings: production, characterization and testing. Phd Thesis 1. Eindhoven (Netherlands): Technische Universiteit Eindhoven.

Wang, K., Zhu, J., Wang, H., Yang, K., Zhu, Y., Qing, Y., et al. (2022). Air plasma-sprayed high-entropy (Y0. 2Yb0. 2Lu0. 2Eu0. 2Er0. 2) 3Al5O12 coating with high thermal protection performance. *J. Adv. Ceram.* 11 (10), 1571–1582. doi:10.1007/s40145-022-0630-2

Wang, X., Cortez, J., Dupuy, A. D., Schoenung, J. M., and Bowman, W. J. (2023). High entropy oxide (Co, Cu, Mg, Ni, Zn) O exhibits grain size dependent room temperature deformation. *Mater. Res. Lett.* 11 (3), 196–204. doi:10.1080/21663831.2022.2135409

Wang, Y. (2022). Processing and properties of high entropy carbides. *Adv. Appl. Ceram.* 121 (2), 57–78. doi:10.1080/17436753.2021.2014277

Wright, A. J., Wang, Q., Ko, S.-T., Chung, K. M., Chen, R., and Luo, J. (2020a). Size disorder as a descriptor for predicting reduced thermal conductivity in medium-and high-entropy pyrochlore oxides. *Scr. Mater.* 181, 76–81. doi:10.1016/j.scriptamat.2020.02.011

Wu, F., Wu, P., Zhou, Y., Chong, X., and Feng, J. (2020). The thermo-mechanical properties and ferroelastic phase transition of RENbO4 (RE= Y, La, Nd, Sm, Gd, Dy, Yb) ceramics. *J. Am. Ceram. Soc.* 103 (4), 2727–2740. doi:10.1111/jace.16926

Wu, M., Liu, Y., Qu, W., Guo, W., Zhang, H., Pei, Y., et al. (2023). Thickness-related failure behaviors of the thermal barrier coatings under thermal gradient cycling. *Surf. Coatings Technol.* 468, 129748. doi:10.1016/j.surfcoat.2023.129748

Wu, Q., Alkemper, A., Lauterbach, S., Hofmann, J. P., and Einert, M. (2024). Fabrication of nanocrystalline high-entropy oxide $CoNiFeCrMnO_{<i>x</i>}$ thin film electrodes by dip-coating for oxygen evolution electrocatalysis. *Energy Adv.* 3, 765–773. doi:10.1039/d4ya00026a

Xing, Q.-W., Xia, S.-Q., Yan, X.-H., and Zhang, Y. (2018). Mechanical properties and thermal stability of $(NbTiAlSiZr)N_{<i>x</i>}$ high-entropy ceramic films at high temperatures. *J. Mater. Res.* 33 (19), 3347–3354. doi:10.1557/jmr.2018.337

Xue, Y., Zhao, X., An, Y., Wang, Y., Gao, M., Zhou, H., et al. (2022). High-entropy (La0. 2Nd0. 2Sm0. 2Eu0. 2Gd0. 2) 2Ce2O7: a potential thermal barrier material with improved thermo-physical properties. *J. Adv. Ceram.* 11 (4), 615–628. doi:10.1007/s40145-021-0563-1

Yan, J., Zhang, L., Liu, J., Li, N., Tamura, N., Chen, B., et al. (2021). Pressure-induced suppression of Jahn–Teller distortions and enhanced electronic properties in high-entropy oxide (Mg0.2Ni0.2Co0.2Zn0.2Cu0.2)O. *Appl. Phys. Lett.* 119 (15). doi:10.1063/5.0067432

Yang, Z.-M., Zhang, K., Qiu, N., Zhang, H.-B., Wang, Y., and Chen, J. (2019). Effects of helium implantation on mechanical properties of (Al0. 31Cr0. 20Fe0. 14Ni0. 35) O high entropy oxide films. *Chin. Phys. B* 28 (4), 046201. doi:10.1088/1674-1056/28/4/046201

Yue, B., Dai, W., Zhang, X., Zhang, H., Zhong, W., Liu, B., et al. (2022). Deformation behavior of high-entropy oxide (Mg,Co,Ni,Cu,Zn)O under extreme compression. *Scr. Mater.* 219, 114879. doi:10.1016/j.scriptamat.2022.114879

Zenkin, S., Gaydaychuk, A., Mitulinsky, A., Bulakh, V., and Linnik, S. (2023). Effect of the MgO addition on the structure and physical properties of the high entropy HfZrCeYO fluorite ceramics. *Coatings* 13 (5), 917. doi:10.3390/coatings13050917

Zenkin, S., Gaydaychuk, A., Mitulinsky, A., and Linnik, S. (2022). Tailoring of optical, mechanical and surface properties of high-entropy Hf-Zr-Ce-Y-O ceramic thin films prepared by HiPIMS sputtering. *Surf. Coatings Technol.* 433, 128164. doi:10.1016/j.surfcoat.2022.128164

Zhang, D., Feng, X., Song, R., Wang, N., and Zhang, Y. (2023a). Investigation on bi-layer coating with La2(Ti0.2Zr0.2Sn0.2Ce0.2Hf0.2)2O7/YSZ prepared by laser cladding. *Ceram. Int.* 49 (7), 10525–10534. doi:10.1016/j.ceramint.2022.11.239

Zhang, D., Feng, X., Song, R., Wang, N., and Zhang, Y. (2023b). An investigation of a La2 (Zr0. 2Ti0. 2Y0. 2Yb0. 2Nb0. 2) 2O7 high entropy oxide coating. *J. Mater. Eng. Perform.*, 1–12. doi:10.1007/s11665-023-08748-x

Zhang, D., Wang, N., Song, R., Zhou, M., Tang, X., and Zhang, Y. (2024). A new TBC material: (La0.2Gd0.2Y0.2Sm0.2Ce0.2)2Zr2O7 high-entropy oxide. *Ceram. Int.* 50 (1), 2490–2500. doi:10.1016/j.ceramint.2023.11.044

Zhao, S. (2021). Lattice distortion in high-entropy carbide ceramics from first-principles calculations. *J. Am. Ceram. Soc.* 104 (4), 1874–1886. doi:10.1111/jace.17600

Zhao, Z., Xiang, H., Dai, F.-Z., Peng, Z., and Zhou, Y. (2019). (TiZrHf) P2O7: an equimolar multicomponent or high entropy ceramic with good thermal stability and low thermal conductivity. *J. Mater. Sci. Technol.* 35 (10), 2227–2231. doi:10.1016/j.jmst.2019.05.030

Zhou, L., Li, F., Liu, J.-X., Hu, Q., Bao, W., Wu, Y., et al. (2020). High-entropy thermal barrier coating of rare-earth zirconate: a case study on (La0. 2Nd0. 2Sm0. 2Eu0. 2Gd0. 2) 2Zr2O7 prepared by atmospheric plasma spraying. *J. Eur. Ceram. Soc.* 40 (15), 5731–5739. doi:10.1016/j.jeurceramsoc.2020.07.061

Zhu, J., Meng, X., Xu, J., Zhang, P., Lou, Z., Reece, M. J., et al. (2021). Ultra-low thermal conductivity and enhanced mechanical properties of high-entropy rare earth niobates (RE3NbO7, RE = Dy, Y, Ho, Er, Yb). *J. Eur. Ceram. Soc.* 41 (1), 1052–1057. doi:10.1016/j.jeurceramsoc.2020.08.070